Journal of Solid State Chemistry 183 (2010) 1550–1554

Contents lists available at ScienceDirect

Journal of Solid State Chemistry

journal homepage: www.elsevier.com/locate/jssc

Local structure of ball-milled $LaNi_5$ hydrogen storage material by Ni K-edge EXAFS

B. Joseph [a], A. Iadecola [a], B. Schiavo [b,c], A. Cognigni [d], L. Olivi [d], G. D'Alì Staiti [b,c], N.L. Saini [a,*]

[a] Dipartimento di Fisica, Università di Roma "La Sapienza", P. le Aldo Moro 2, 00185 Roma, Italy
[b] Istituto Tecnologie Avanzate, Base di ASI Luigi Broglio, Strada Statale 113, Trapani 9100, Italy
[c] Dipartimento di Fisica e Tecnologie Relative, Università di Palermo, Viale delle Scienze, Palermo 90100, Italy
[d] Elettra, Sincrotrone Trieste, Strada Statale 14, Km 163.5, Basovizza, Trieste, Italy

ARTICLE INFO

Article history:
Received 2 October 2009
Received in revised form
15 April 2010
Accepted 25 April 2010
Available online 13 May 2010

Keywords:
Hydrogen storage materials
Nanostructuring
Local structure
Atomic disorder

ABSTRACT

Local structure of the nanostructured $LaNi_5$ hydrogen storage alloys, prepared by ball-milling, has been studied using Ni K-edge extended X-ray absorption fine structure spectroscopy. Results indicate that the ball-milling up to 100 h results in the production of nanoparticles characterized by large atomic disorder and slightly reduced unit-cell volume, compared to the bulk $LaNi_5$. High temperature annealing appears to help in partial recovery of atomic order in the ball-milled samples; however, long-time ball-milled samples retain large disorder even after the high temperature annealing. The results suggest that the large disorder and the reduced unit-cell volume might be causing a higher energy-barrier for the hydride-phase formation in the long time ball-milled $LaNi_5$ powders.

1. Introduction

Hydrogen is hailed as a non-polluting synthetic fuel that could replace oil, especially for the transport applications [1]. $LaNi_5$ is one of the well known hydrogen absorption materials with remarkable reversible hydrogenation properties at room temperature. Many attempts have been made to develop new hydrogen absorption materials superior to $LaNi_5$, but very few of those could succeed. Nanostructuring is one of the possible approaches to improve the hydrogenation properties of materials [2,3]. For the synthesis of nanomaterials, techniques like ball-milling [4] are preferred due to the easy scale-up possibilities from laboratory to industrial levels. In fact, ball-milling is the preferred nanostructuring tool for the hydrogen storage materials [3,5]. However, nanomaterials of $LaNi_5$ produced by ball-milling are found to exhibit inferior hydrogen storage properties [6]. In order to develop suitable nanomaterials with superior hydrogen absorption properties, it is of prime importance to understand the changes in the electronic and the local structural properties of this classical hydrogen storage material in the nanoparticle form.

Extended X-ray absorption fine structure (EXAFS) spectroscopy is a site selective method, providing information on the local atomic distribution around a selected absorbing atom through photoelectron scattering [7,8]. Apart from its traditional applications in several fields of material science [7,9], recently, this technique has also been extensively used for the local structure studies of several nanomaterial systems [10–12]. Here, we have exploited the Ni K-edge EXAFS spectroscopy to make a systematic study of the local structure around the Ni atom in $LaNi_5$, by measuring a series of samples where the particle size is varied through ball-milling involving milling times up to 100 h. The results suggest that the unit-cell volumes of the long-time ball-milled $LaNi_5$ powders are slightly smaller than the bulk, consistent with an expected lattice-parameter reduction for the nanoparticles. The Debye Waller factors (DWFs) measuring the mean square relative displacements (MSRDs) of the bond lengths are found to be substantially higher for the ball-milled samples, indicating a substantial increase in the atomic disorder with milling. Interestingly, EXAFS data indicated that the long-time ball-milled powders are retaining large disorders even after the high temperature annealing. Larger MSRDs with reduced unit-cell volumes for the $LaNi_5$ nanoparticles produced by ball-milling may cause a higher energy-barrier for the hydride phase formation in this system.

2. Experimental details

Hydrogen storage grade $LaNi_5$ samples from Sigma-Aldrich were used for the present study. Ball-milling of these samples were carried out using a FRITSCH miller (Pulverisette 6), using

* Corresponding author.
E-mail address: Naurang.Saini@roma1.infn.it (N.L. Saini).

0022-4596/$ - see front matter © 2010 Elsevier Inc. All rights reserved.
doi:10.1016/j.jssc.2010.04.034

stainless steel vial and balls at 240 rotations per minutes with a ball to powder ratio around 10. Milling was carried out in cycles of 20 min milling time and 20 min pause time to avoid the heating of the sample during the milling process. Samples were prepared with milling times 2, 20 and 100 h. All the sample-handlings were carried out inside an Ar filled glove box (Mbraun) to avoid possible contacts with air. To study the annealing effects, a part of the 100 h ball-milled sample was annealed at 730 °C for 1 h while the 20 h ball-milled sample was annealed at 500 °C for 30 min. The annealings were performed under high vacuum ($\sim 10^{-6}$ mbar). The samples were analyzed by powder X-ray diffraction (XRD) measurements, using an in-house X-ray source with Cu $K\alpha$ radiations.

The X-ray absorption measurements were made at the XAFS beamline of the Elettra synchrotron radiation facility, Trieste, where the synchrotron radiation emitted by a bending magnet source was monochromatized using a double crystal Si(111) monochromator. The Ni K-edge EXAFS measurements were made at 80 and 300 K in the transmission mode using three ionization chambers mounted in series for simultaneous measurements on the sample and a reference. Prior to the EXAFS measurements, the samples were characterized for the hydrogen absorption properties by measuring the pressure composition isotherms using an automated PCT apparatus (HyEnergy) [6]. As a routine experimental approach, several X-ray absorption scans were collected to ensure the reproducibility of the spectra, in addition to the high signal to noise ratio. Standard procedure was used to extract the EXAFS oscillations from the absorption spectrum [8]. Rietveld refinement of the XRD data was carried out using the MAUD package making it possible to perform simultaneous structure and size-strain analysis [13].

3. Results and discussion

3.1. Ball-milling time dependence

Fig. 1 shows EXAFS oscillations (multiplied by k^3), extracted from room temperature Ni K-edge X-ray absorption spectra, measured on the $LaNi_5$ powders with variable ball-milling time. The EXAFS amplitude decreases with increasing milling time. The decrease is substantial for the 20 h milled powders compared to the bulk (as-prepared) and the 2 h milled samples, albeit, the changes from 20 to 100 h is not that significant. Incidentally such a reduction of the EXAFS amplitude is known to occur in several systems when the bulk is nanostructured. For example, nanocrystalline Fe prepared by ball-milling [14], substrate free Pd nanoparticles prepared by evaporation [15], Ge [12] and Pt [11] nanoclusters synthesized by ion implantation and Au nanoparticles prepared by solvated metal atom dispersion [10] or consecutive evaporation of Au and Mylar [16], etc. are found to show a systematic damping of the EXAFS oscillations with reduction of the particle size.

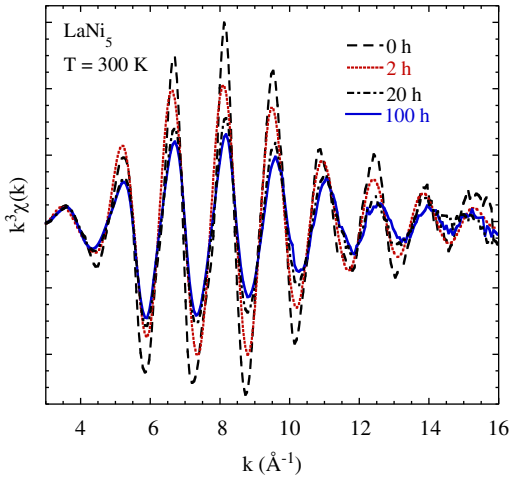

Fig. 1. (color-online) EXAFS oscillations (multiplied by k^3) extracted from room temperature Ni K-edge absorption spectra of $LaNi_5$ with different ball-milling. Legends indicate milling times, where 0 h correspond to the unmilled (bulk) sample. With increasing milling time the EXAFS oscillations are getting damped indicating an enhanced atomic disorder.

Fig. 2 shows the XRD patterns of the bulk and the milled samples. As expected, the XRD pattern for the bulk sample is identical to the one reported in the literature [20]. The $LaNi_5$ crystal structure is hexagonal $CaCu_5$-type with $P\ 6/mmm$ symmetry [17–20]. Inset in Fig. 2 shows the crystal structure of $LaNi_5$. The lattice parameters of the bulk sample obtained from the XRD analysis are consistent with earlier reports [17–20]. The structural parameters obtained from the refinement are given in Table 1. It is found that the 20 and 100 h milled samples have all the diffraction peaks as the bulk. However, the peak intensities are found to be progressively damped with the increasing milling time. There is also a large broadening of the peaks. Such features in the XRD profiles are typical of the nanoparticles. The estimated crystallite sizes for the 20 and 100 h milled samples are also included in Table 1. Although, the milled samples are found to have identical crystal structure as the bulk, the corresponding lattice parameters are found to be slightly different, in particular, the lattice parameters a and b are found to become progressively shorter with increasing milling time (Table 1).

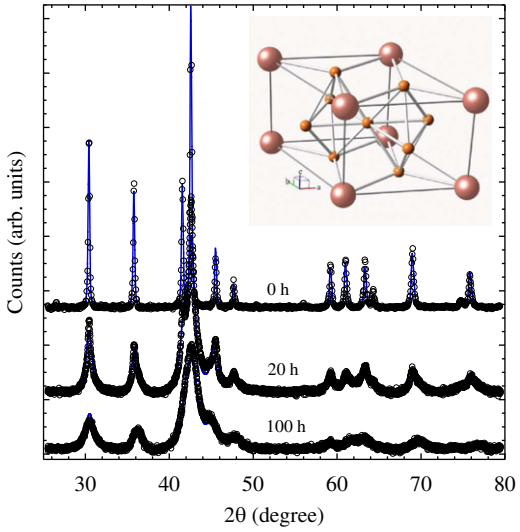

Fig. 2. (color-online) XRD profiles of the 0, 20 and 100 h ball-milled $LaNi_5$ samples. The 0 h represents the bulk (unmilled) sample. Rietveld refinement results are included as solid lines. With increasing milling time, diffraction peaks are getting broader with reduced intensity. The inset shows the crystal structure of $LaNi_5$ where the larger spheres represent the La atoms.

Table 1
Results of the XRD Rietveld analysis.

Sample	*Rwp*(%)	$a=b$ (Å)	c (Å)	Crystallite size (nm)
bulk	1.45	5.0160(4)	3.9836(3)	–
20 h	4.9	5.0106(6)	4.001(8)	12.3(±3)
100 h	20	4.975(3)	4.036(4)	8.3(±5)

Space group $P\ 6/mmm$, $\alpha=\beta=90, \gamma=120$. La (site 1*a*) *x* 0.0, *y* 0.0, *z* 0.0; Ni (site 2*c*) *x* $\frac{1}{3}$, *y* $\frac{2}{3}$, *z* 0.0; Ni (site 2*c*) *x* $\frac{1}{2}$, *y* 0.0, *z* $\frac{1}{2}$.

In the crystal unit cell the La atoms occupy the 1*a* site, whereas Ni atoms have two different positions, viz. 3*g* and 2*c*. The unit cell of $LaNi_5$ contains one La atom, three Ni atoms at 3*g* site and two Ni atoms at 2*c* site. Model of the $LaNi_5$ crystal structure is shown in the inset of Fig. 2. Corresponding structural parameters are given in Table 1. This structural configuration gives rise to three Ni–Ni near-neighbor distances (~2.46, ~2.5, and ~2.85 Å) and two Ni–La near-neighbor distances (~2.9, and ~3.2 Å). For a proper treatment of the Ni K-edge EXAFS data of $LaNi_5$, it is important to consider the presence of two distinct Ni sites in the crystal structure. From the Ni 3*g* site, the first three near neighbors are four Ni atoms each at ~2.46 and ~2.51 Å and four La atoms at ~3.2 Å, whereas from the Ni 2*c* site, the first three near neighbors are six Ni atoms at ~2.46 Å, two Ni atoms at ~2.89 Å and two La atoms at ~2.89 Å. As the EXAFS signal from the two Ni sites cannot be distinguished, we have adopted a method of weighted average from the two Ni site contributions to model the data. It is to be recalled that the earlier EXAFS studies on this system have overlooked this fact and assumed only an average Ni–Ni distance for the analysis of the EXAFS data [23–25].

Fig. 3 shows the Fourier transforms (FTs) of the EXAFS data measured at 80 and 300 K with varying milling time. FTs were performed between the *k* range 2.9 and 17 $Å^{-1}$. The main peak in the FT (in Fig. 3 between 1.3 and 3.4 Å) is mainly due to the Ni–Ni and Ni–La single scatterings. These corresponds to the above discussed three near neighbor contributions from the two Ni sites. At both 80 and 300 K, the amplitude of the main peak in the FT are found to decrease with increasing milling time. To obtain quantitative information, we have modelled the EXAFS using the WINXAS package [21] with calculated phase and amplitude functions from the FEFF7 [22]. The EXAFS amplitude depends on several factors and could be given by the following general equation [8]:

$$\chi(k) = \sum_i \frac{N_i S_0^2}{kR_i^2} f_i(k,R_i) e^{-2R_i/\lambda} e^{-2k^2\sigma^2} \sin[2kR_i + \delta_i(k)] \quad (1)$$

where N_i is the number of neighboring atoms at a distance R_i. S_0^2 is the passive electrons reduction factor, $f_i(k,R_i)$ is the backscattering amplitude, λ is the photoelectron mean free path, and σ_i^2 is the correlated Debye–Waller factor (DWF), measuring the mean square relative displacements (MSRDs) of the photoabsorber–backscatterer pairs. Apart from these, the photoelectron energy origin E_0 and the phase shifts δ_i should be known. We have used conventional procedure to analyze the EXAFS signal [8] due to five shells (three Ni–Ni and two Ni–La distances). Except the radial distances R_i and the corresponding DWFs, σ_i^2, all other parameters were kept fixed in the least squares fit. The co-ordination numbers were fixed to the weighted average of the same from the two Ni sites. The passive electron reduction factor S_0^2 was fixed to 1. The E_0 was fixed to −8.9 eV. The number of independent data points, $N_{ind} \simeq (2\Delta k \Delta R)/\pi$ [8] was 18 for the present analysis ($\Delta k = 14.1$ $Å^{-1}$ and $\Delta R = 2.1$ Å). The obtained fits are included in Fig. 3 as solid lines.

Fig. 4 shows the near neighbor distances resulting from the best fit with the five shells for $T = 80$ and 300 K. Here it is worth mentioning that earlier local structure studies on the $LaNi_5$ system [23–26] have adopted different approach considering only a single Ni–Ni distance extracting a mean Ni–Ni distance with an average DWF neglecting the actual atomic distribution around the photoabsorber. However, diffraction results as a starting point yield more realistic information on local structural parameters. All

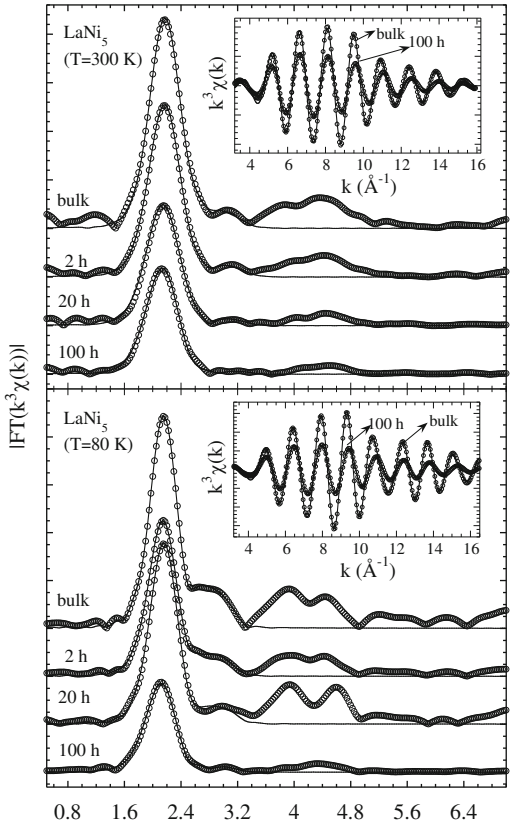

Fig. 3. Fourier transforms (FTs) of the Ni K-edge EXAFS oscillations measured at 300 K (upper panel) and 80 K (lower panel) revealing the partial atomic distribution around the Ni. FTs are performed between $k_{min} = 2.9$ $Å^{-1}$ and $k_{max} = 17$ $Å^{-1}$ using a Gaussian window. Model fits with five shells (solid line) are also included. Insets show fit in the *k*-space (filtered EXAFS oscillations corresponding to 1.3 – 3.4 Å) for the bulk and the 100 h milled samples.

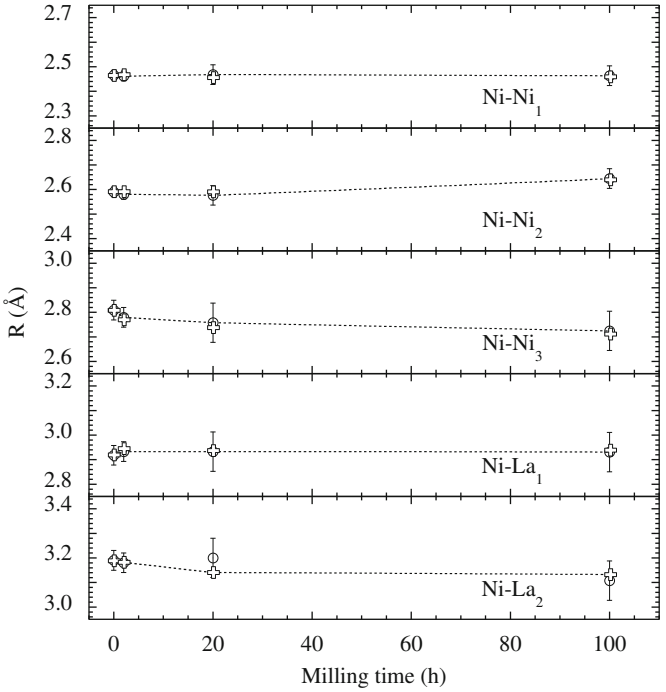

Fig. 4. Near-neighbor distances obtained from a five shell fit to the Ni K-edge EXAFS (shown in Fig. 3). Open circles and crosses are data from 80 and 300 K, respectively. The Ni–Ni_1 and Ni–La_1 distances seem to remain constant with milling time. Ni–Ni_3 and Ni–La_2 show a decrease, whereas Ni–Ni_2 shows an increase indicating an overall reduction in the unit-cell volume for the 100 h milled sample. The dotted line is a guide to the eyes and error bars represent the average uncertainties evaluated using correlation maps.

the near-neighbor distances obtained from the fit for the bulk sample are quite similar to those expected from the diffraction data (the three Ni–Ni distances ~2.45, ~2.5 and ~2.85 Å and the two Ni–La distances ~2.9, and ~3.2 Å). The near neighbor distances show an interesting variation with ball-milling time (Figs. 4 and 5). While the distances corresponding to 2.4 Å Ni–Ni and 2.9 Å Ni–La distance are found to remain constant with increasing ball-milling, other distances, seem to differ for the 100 h milled sample compared to the bulk. The 2.5 Å Ni–Ni seems to show a slight increase for the 100 h milled sample while the 2.8 Å Ni–Ni and 3.2 Å Ni–La show a reduction. This means that there is a reduction in the unit-cell volume for the 100 h milled sample. The XRD analysis (Table 1) also indicates a similar result. The variation in the distances corresponding to the different shells is found to have the same trend at both 80 and 300 K, with hardly any change due to temperature within the uncertainties. Using the La L_3-edge EXAFS, it is possible to study the Ni–La bond-distributions of this system. In fact our studies using the La L_3-edge EXAFS on this system showed that with increasing ball-milling time, the 2.9 Å Ni–La distance remains constant while 3.2 Å Ni–La shows a decrease [27]. The variation of the Ni–La distances observed in the present case are consistent with the above studies. The decrease of near neighbor distances with the ball-milling is consistent with the decreased size of the crystallites having dimensions in the range of nanometers. The fact that the distances corresponding to the different shells do not show a similar change with the ball-milling time recalls the anisotropy of the bond-strengths determined recently in a study of elastic constants of the $LaNi_5$ [28].

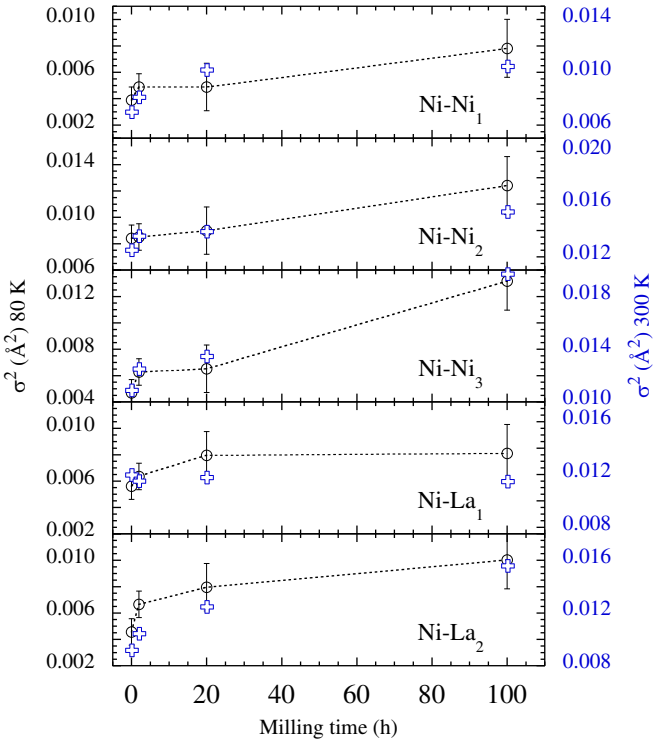

Fig. 5. (color-online) The MSRDs of different atomic pairs obtained from the five shell fit to the Ni K-edge EXAFS (shown in Fig. 3). Open circles and crosses are data at 80 and 300 K, respectively. The ordinate corresponding to 80 K is shown in the left and that corresponding to 300 K is shown in the right. As expected, the MSRD values at 300 K are higher than that at 80 K for all the atomic pairs. An increased atomic disorder with ball-milling is clear from the larger values of MSRDs for the milled samples. The dotted line is a guide to the eyes and error bars represent the average uncertainties evaluated using correlation maps. Error bars are avoided for the 300 K for the clarity in presentation.

Fig. 5 shows the MSRDs of the bond lengths revealing the atomic level disorder (static and dynamic) in the $LaNi_5$ as a function of ball-milling time obtained from the modelling of the EXAFS data. The MSRDs for all the atomic shells show clear increase with milling time, revealing a global increase of the atomic disorder. The behavior of the MSRDs with milling time was found to be same at both 80 and 300 K (Fig. 5). The observed disorder seems to be typical of nanoparticles [10,11,14–16,29]. Indeed, going from the bulk to nanomaterials, an enhancement in the MSRDs is observed for several systems [10–12,15,16]. It should be mentioned that some earlier EXAFS studies on nanoparticles of Ge, Au, Pd and Fe have discussed the large damping of the EXAFS amplitude as being due to the reduction of near neighbor atoms in the nanoparticles in comparison to the bulk. In the present analysis we have fixed near neighbor atoms, necessary to reduce correlation between different parameters to get meaningful values for the interatomic distances and the corresponding MSRDs. Moreover, the MSRDs include both static and dynamic disorder in the system including vacancies at the near neighbor sites and lattice distortions, therefore consistent with the earlier experiments revealing reduced near neighbors with the nanostructuring. Studies using the La L_3-edge EXAFS on the same system indicated a similar behavior of the MSRDs of the La–Ni bonds [27].

3.2. *Effect of annealing on ball-milled samples*

Let us discuss the effect of annealing on the ball-milled samples of the $LaNi_5$. We have studied the 20 and 100 h ball-milled samples before and after annealing. Fig. 6 shows the FTs of the room temperature Ni K-edge EXAFS data for the 20 and 100 h milled-and-annealed samples, along with the data for the bulk sample. For the 20 h milled powders, annealing seems to restore both the distances as well as the average atomic order (Fig. 6). This is consistent with the earlier observations on ball-milled Fe, in which the annealing is found to restore the EXAFS amplitude for milling times up to 32 h and explained as due to the annealing induced reduction in the disorder formed by milling [14]. On the other hand, for the 100 h ball-milled sample, the high temperature annealing is not enough to restore the interatomic distances and the atomic order.

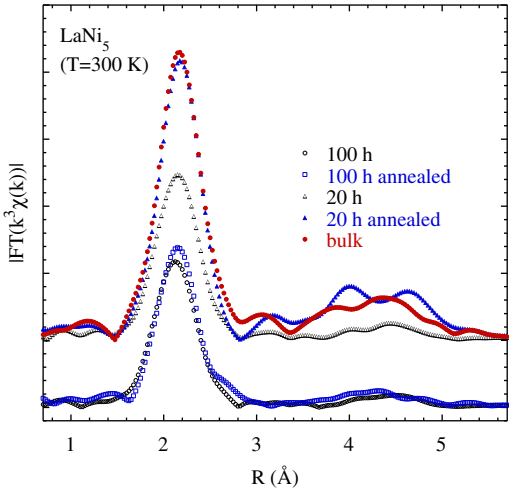

Fig. 6. (color-online) Fourier transforms (FTs) of the room temperature Ni K-edge EXAFS oscillations measured before (open circles) and after (open squares) the high temperature annealing. There is a substantial reduction in the atomic disorder for the 20 h ball-milled sample after annealing, while the annealing of the 100 h ball-milled sample hardly affects the atomic disorder. The FT of the bulk sample is shown for comparison (filled circles).

As far as the hydrogen uptake capacity, it is found that the capacity decreases gradually with an increasing ball-milling time; however, the capacity could be regained by the high temperature annealing [6]. It should be recalled that after annealing, the equilibrium plateau pressure, where the continuous conversion of the α ($LaNi_5$) to β ($LaNi_5H_6$) phase occurs, is found to be highest for the 100 h ball-milled samples [6]. A decrease in the unit-cell volume and an increase in the MSRDs corresponding to the near-neighbor bond lengths (i.e., atomic disorder) may cause a higher energy-barrier for the H-induced unit-cell doubling [19] involving the formation of Ni–H bonds [23] in the $LaNi_5$. Such a situation can account for the observed large plateau pressure [6] for the 100 h milled-and-annealed powders.

4. Summary

In summary, we have studied the local structure of $LaNi_5$ hydrogen storage alloys using Ni K-edge EXAFS. Results indicate that the unit-cell volume of the long-time ball-milled $LaNi_5$ powders is slightly smaller compared to the bulk. These results are consistent with XRD results which show changes in the lattice-parameters of the long-time ball-milled samples. The MSRDs of the bond lengths are found to increase with increasing ball-milling time, indicating an increased atomic disorder with the milling time. High temperature annealing is found to be capable of reducing the disorder in milled samples for milling times up to 20 h. However, the long time ball-milled samples (milled for 100 h) retain a large disorder even after the high temperature annealing. The relatively large values of MSRDs together with a slightly reduced unit-cell volume for the nanoparticles may cause a higher energy-barrier for the hydride phase formation in case of long-time ball-milled $LaNi_5$ powders.

Acknowledgments

The XAFS measurements were carried out under the proposal number 20090071 at the XAFS Beamline of the Elettra Synchrotron Facility, Trieste, Italy. One of us (B.J.) would like to acknowledge the MIUR (Italy) for a fellowship under the Italy–India bilateral program. Authors thank Dr. Alessandro Latini of Dip. di Chimica, La Sapienza, Roma, for the XRD data collection.

References

[1] L. Schlapbach, Nature 460 (2009) 809;
D. Chandra, J. Reilly, R. Chellappa, JOM J. Miner. Met. Mater. Soc. 58 (2006) 26;
L. Schlapbach, A. Zuttel, Nature 414 (2001) 353.
[2] M. Fichtner, Adv. Eng. Mater. 7 (2005) 443;
A.S. Arico, P. Bruce, B. Scrosati, J.-M. Tarascon, W. van Schalkwijk, Nat. Mater. 4 (2005) 366;
B. Vincent, R. Gregg, D. Mildred, C. Gang, Int. J. Energy Res. 31 (2007) 637.
[3] A. Zaluska, L. Zaluski, J.O. Strötom-Olsen, J. Alloys Compd. 288 (1999) 217;
M. Dornheim, S. Doppiu, G. Barkhordarian, U. Boesenberg, T. Klassen, O. Gutfleisch, R. Bormann, Scr. Mater. 56 (2007) 841.
[4] C. Suryanarayana, Prog. Mater. Sci. 46 (2001) 1.
[5] M. Dornheim, N. Eigen, G. Barkhordarian, T. Klassen, R. Bormann, Adv. Eng. Mater. 8 (2006) 377.
[6] B. Joseph, B. Schiavo, J. Alloys Compd. 480 (2009) 912.
[7] P.A. Lee, P.H. Citrin, P. Eisenberger, B.M. Kincaid, Rev. Modern Phys. 53 (1981) 769.
[8] R. Prins, D. Koningsberger (Eds.), X-ray Absorption: Principles, Applications, Techniques of EXAFS, SEXAFS, XANES, Wiley, New York, 1988.
[9] See for example a review by A. Bianconi, N.L. Saini, Struct. Bonding 114 (2005) 287.
[10] T. Comaschi, A. Balerna, S. Mobilio, Phys. Rev. B 77 (2008) 075432.
[11] R. Giulian, L.L. Araujo, P. Kluth, D.J. Sprouster, C.S. Schnohr, G.J. Foran, M.C. Ridgway, J. Phys. Condens. Matter (2009) 155302.
[12] L.L. Araujo, R. Giulian, D.J. Sprouster, C.S. Schnohr, D.J. Llewellyn, P. Kluth, D.J. Cookson, G.J. Foran, M.C. Ridgway, Phys. Rev. B 78 (2008) 094112.
[13] L. Lutterotti, P. Scardi, J. Appl. Phys. 23 (1990) 246;
L. Lutterotti, S. Gialanella, Acta Mater. 46 (1998) 101.
[14] A. Di Cicco, M. Berrettoni, S. Stizza, E. Bonetti, G. Cocco, Phys. Rev. B 50 (1994) 12386.
[15] L. Chih-Ming, H. Tsu-Lien, H. Yen-Heng, W. Kung-Te, T. Mau-Tsu, L. Chih-Hao, C.T. Chen, Y.Y. Chen, Phys. Rev. B 75 (2007) 125426.
[16] A. Balerna, E. Bernieri, P. Picozzi, A. Reale, S. Santucci, E. Burattini, S. Mobilio, Phys. Rev. B 31 (1985) 5058.
[17] A. Percheron-Gugan, C. Lartigue, J.C. Achard, P. Germi, F. Tasset, J. Less-Common Met. 74 (1980) 1.
[18] P. Thompson, J.J. Reilly, L.M. Corliss, J.M. Hastings, R. Hempelmann, J. Phys. F Met. Phys. 16 (1986) 675.
[19] K. Tatsumi, I. Tanaka, H. Inui, K. Tanaka, M. Yamaguchi, H. Adachi, Phys. Rev. B 64 (2001) 184105;
Y. Yu, H. Han, Y. Zhao, W. Xue, T. Gao, Solid State Commun. 148 (2008) 1.
[20] Y. Nakamura, K. Oguro, I. Uehara, E. Akiba, Int. J. Hydrogen Energy 25 (2000) 531.
[21] T. Ressler, J. Synch. Radiat. 5 (1998) 118.
[22] S.I. Zabinsky, J.J. Rehr, A.L. Ankudinov, R.C. Albers, M.J. Eller, Phys. Rev. B 52 (1995) 2995.
[23] M. Matsuura, K. Asada, K. Konno, M. Sakurai, J. Alloys Compd. 390 (2005) 31.
[24] O. Palumbo, C. Castellano, A. Paolone, F. Cordero, R. Cantelli, Y. Nakamura, E. Akiba, J. Alloys Compd. 433 (2007) 33.
[25] H. Sakaguchi, T. Suenobu, K. Moriuchi, M. Yamagami, T. Yamaguchi, G. Adachi, J. Alloys Compd. 221 (1995) 212;
H. Sakaguchi, T. Suenobu, T. Tsujimoto, K. Moriuchi, H. Kanai, S. Yoshida, G. Adachi, Jpn. J. Appl. Phys. 32 (Suppl. 32-2) (1993) 679–681;
H. Sakaguchi, T. Tsujimoto, K. Moriuchi, Kiyoaki, H. Kanai, S. Yoshida, G. Adachi, Jpn. J. Appl. Phys. 32 (Suppl. 32-2) (1993) 682–684;
T. Suenobu, H. Sakaguchi, G. Adachi, H. Kanai, S. Yoshida, J. Alloys Compd. 190 (1993) 273.
[26] J.E. Bonnet, P. Dantzer, H. Dexpert, J.M. Esteva, R. Karnatak, J. Less-Common Met. 130 (1987) 491.
[27] B. Joseph, A. Iadecola, B. Schiavo, A. Cognigni, L. Olivi, N.L. Saini, Large atomic disorder in nanostructured LaNi5 alloys: A La L3-edge extended X-ray absorption fine structure study, J. Phys. Chem. Solids (2010), doi:10.1016/j.jpcs.2010.03.008.
[28] T. Kazuyoshi, T. Isao, T. Katsushi, I. Haruyuki, Y. Masaharu, A. Hirohiko, M. Masataka, J. Phys. Condens. Matter 15 (2003) 6549.
[29] B. Gilbert, F. Huang, H. Zhang, G.A. Waychunas, J.F. Banfield, Science 305 (2004) 651.